Materials Science & Engineering A 856 (2022) 144031

Contents lists available at ScienceDirect

Materials Science & Engineering A

journal homepage: www.elsevier.com/locate/msea

Influence of precipitate and grain sizes on the brittle-to-ductile transition in Fe–Al–V bcc-L2$_1$ ferritic superalloys

P.A. Ferreirós [a,b,c,*], U.A. Sterin [b,c], P.R. Alonso [b], A.J. Knowles [a], G.H. Rubiolo [b,c]

[a] School of Metallurgy and Materials, University of Birmingham, Birmingham, B15 2TT, UK
[b] Gerencia Materiales (GAEN), Comisión Nacional de Energía Atómica (CNEA) and Instituto Sabato, Universidad Nacional de San Martín (UNSAM), Av. Gral. Paz 14919, San Martín, B1650KNA, Buenos Aires, Argentina
[c] Consejo Nacional de Investigaciones Científicas y Técnicas (CONICET), Godoy Cruz 2290, Ciudad Autónoma de Buenos Aires, C1425FQ2B, Argentina

ARTICLE INFO

Keywords:
Fe-Al-V
Superalloy
Brittle-to-ductile transition
Ageing
Precipitate size
Impact test

ABSTRACT

The limiting factors to achieving a wide application of bcc-superalloys are the high brittle-to-ductile transition temperatures (BDTT). The understanding of the mechanisms controlling the BDTT and how to optimise the microstructure in polycrystalline bcc-superalloys remains a concern today.

In the present work, the influence of grain and coherent precipitates sizes on strength and brittle-to-ductile transition temperature (BDTT) are studied in a $Fe_{78}Al_{10}V_{12}$ (A2+L2$_1$) ferritic superalloy, toward application in high-efficiency power plants. Additionally, the A2 matrix behaviour was evaluated in a derived single-phase-bcc $Fe_{84}Al_8V_8$ alloy. Thermal ageing and coarsening treatments were applied to produce samples with different precipitate and grain sizes. Tensile tests were carried out at different temperatures and strain rates to assess the variation of the yield stress. Charpy impact tests were used to measure the BDTT in both alloys, which was substantially reduced with grain size refinement, and precipitate coarsening. It was found that the increase in cleavage stress by precipitation strengthening follows the same behaviour that the increase in yield stress for coherent strengthened bcc-superalloys. Integration into a physical-based model, which identified a novel interplay with cleavage stress, provides enhanced BDTT predictive capability for ferritic superalloys.

1. Introduction

Nowadays, the most efficient fossil-energy power plants operate with a main steam temperature of 580–600 °C and steam pressure of 24–35 MPa. The thermal efficiency could be increased by ~ 5.7% by raising the steam temperature to 650 °C [1]. The 9–12 %Cr ferritic steels (T/P91, T/P92 and T/P911) are the most widely used materials in fossil power plants, but their highest service temperature is limited to ~ 600 °C due to consideration of its resistance to creep and corrosion [2]. Therefore, great effort has been made to develop high-temperature materials to meet the rising requirements of steam turbines in high-efficiency power plants [3]. Among others, ferritic iron-aluminide alloys with strengthening intermetallic phases have been identified as promising candidates [4,5]. In particular, the strengthening of a ductile ferritic matrix by coherent intermetallic precipitation have been explored in many Fe–Al-base ternary systems [6–11], showing advantageous mechanical properties over conventional ferritic steels, mainly regarding high-temperature strength and creep resistance.

However, a major drawback was the high brittle-to-ductile transition temperature (BDTT) often observed in the precipitate-strengthening Fe–Al base alloys as shown in Table 1 [7,12–14]. A proper comparison of BDTT values is complex due to variation or non-reporting of microstructural parameters, for example, the $Fe_{69}Al_{21}Ti_{10}$ alloy showed a BDTT drop following precipitate coarsening [7], while Fe–Al–Mo alloys did not display a change in BDTT with changing the volume fraction [13], and in Fe–Al–Ta the authors attribute the BDTT drop to grain size reduction [14].

Understanding the mechanisms that control BDTT in bcc polycrystalline alloys remains a concern today [15–19]. Armstrong's analysis [20], based on previous steel tests [21], explained the BDTT decrease due to grain refinement through the inequality observed in the yield stress (σ_y) and cleavage stress (σ_c) dependence on grain size. Ferritic Fe_2AlTi(L2$_1$)-strengthened alloys have shown a BDTT decrease from 750 °C to 500 °C by reduction of the grain size from 100 to 10 μm

* Corresponding author. Engineering North Campus, Metallurgy & Materials, Elms Road, University of Birmingham, Edgbaston, Birmingham, B15 2SE, United Kingdom.
E-mail address: p.ferreiros@bham.ac.uk (P.A. Ferreirós).

https://doi.org/10.1016/j.msea.2022.144031
Received 15 June 2022; Received in revised form 15 September 2022; Accepted 16 September 2022
Available online 21 September 2022
0921-5093/© 2022 The Authors. Published by Elsevier B.V. This is an open access article under the CC BY license (http://creativecommons.org/licenses/by/4.0/).

[22]. In precipitation-strengthened alloys, another method to reduce the BDTT is to increase the precipitate size to that above peak hardening (over-ageing). Ferritic NiAl-strengthened alloys have shown a BDTT decrease from 625 °C to 425 °C by over-ageing [4]. Often, this phenomenon is explained by the expected decrease of σ_y with precipitate coarsening by over-ageing while σ_c remains unchanged. However, there is no evidence that σ_c would not vary significantly in this type of ferritic-strengthened alloys. Therefore, experiments that demonstrate the link of σ_c with precipitate sizes are required to expand the current models of BDTT.

We have reported promising mechanical properties of a model $Fe_{76}Al_{12}V_{12}$ (at. %) A2+$L2_1$ ferritic superalloy regarding compressive yield strength, ~ 800/600 MPa at 600/650 °C respectively [12], however, it has a high BDTT as shown in Table 1. Given our knowledge about the industrial hot-forming processing, such as forging and working of the cast microstructure, followed by ageing treatment of this ferritic superalloy, we can prepare samples to verify if the reduction in the grain size of the disordered matrix and precipitate coarsening may lead to a marked decrease of its BDTT.

In this work, we use a model $Fe_{76}Al_{10}V_{12}$ (at. %) A2+$L2_1$ ferritic superalloy to study the synergy between grain and precipitate size to shift the value of its BDTT. Further, considering the matrix phase composition [23], a $Fe_{84}Al_8V_8$ alloy was also produced to evaluate the A2 solid solution. The cleavage stress is estimated by the relationship $\sigma_c = Q\,\sigma_{y(NDT)}$, where $\sigma_{y(NDT)}$ is the yield stress at general yield measured at the nil ductility temperature (*NDT*) and Q is a plastic stress intensification factor due to triaxial stress state below the root of V-notch in Charpy testing [20,21]. In this way, we were able to evaluate the change in cleavage stress between a monophasic and a biphasic alloy, whose connecting phase has the same crystal structure and chemical composition, and thus access a powerful strategy to minimize the BDTT of this ferritic superalloy.

2. Materials and methods

Two alloys were prepared by air induction melting using mild steel SAE 1005 plates (0.05 %C), aluminium ingots (99.9%) and ferrovanadium lumps (80V–20Fe, 0.09 %C) (wt.%). Cylindrical ingots (Ø 50 × 80 mm^2) of 2 kg were cast into sand moulds with an open riser volume of 50%. The As-cast ingots were solution heat-treated at 1100 °C for 4 h with Ar flow. Table 2 shows the average of chemical compositions measured by Wavelength Dispersive X-ray Fluorescence (WDXRF) on a Bruker S8-Tiger. The conditioned ingots were forged up to 20 × 20 mm^2 section in an open-die with a 100 kg pneumatic hammer Bêché & Grohs L3 (200 hits/min and 1.62 kJ impact energy) at temperatures between 1100 °C and 900 °C (A2 single-phase field [24]). The square section bars were heated in Ar flow at 970 °C and then hot-rolled at 54 rpm (roll Ø210 mm) in a 50 HP Krupp. The bars were rolled up to 2.8 mm thickness in five steps with an incremental true strain of ε = 26, 33, 40, 47 and 52 %. Rolled samples of the $Fe_{78}Al_{10}V_{12}$ alloy were aged under vacuum at 700 °C for 0.37 h (peak hardening condition, PHC [11]), 5 h and 72 h (over-aged conditions). Samples with an additional grain growth (GG) isothermal treatment at 1100 °C/2 h and further PHC ageing were performed. Table 3 summarizes the thermal treatments performed on each sample.

Table 2
Chemical compositions by WDXRF (at. %). The error represents the standard deviation obtained from different zones of the samples.

Alloy	Phases	Fe	Al	V	Si	Mn
$Fe_{78}Al_{10}V_{12}$	A2+$L2_1$	77.0 ± 0.8	10.0 ± 0.5	12.2 ± 0.5	0.4 ± 0.01	0.4 ± 0.01
$Fe_{84}Al_8V_8$	A2	82.6 ± 0.7	8.5 ± 0.5	8.4 ± 0.5	0.2 ± 0.01	0.2 ± 0.01

Samples for metallographic inspection were mounted on conductive Bakelite. The surfaces were prepared by semi-automatic grinding equipment using silicon carbide paper from 120 to 4000 grit sizes and final polishing with 60 nm colloidal silica suspension for 30 min with low force (10 N). Scanning Electron Microscopy (SEM) was performed in a Jeol 7000F with a Schottky type field-emission gun, Oxford Inca EDS and Electron Backscatter Diffraction (EBSD) detectors. The observations were done using a working distance (WD) of 10 mm, an acceleration voltage of 20 kV and for EBSD mappings: the WD was doubled, step sizes of 1.08 μm and 0.54 μm with resolutions of 1024 and 2048 were applied for the largest and smallest grain sizes respectively. Fig. 1 shows the microstructure of the $Fe_{78}Al_{10}V_{12}$ samples. To study the vanadium-rich carbides, these were revealed by etching the ferritic matrix with Kroll's reagent (Fig. 1c). The $L2_1$ precipitate sizes were measured on electropolished thin foils in a Transmission Electron Microscopy (TEM) Philips CM200 (Fig. 1b) operated at 200 kV. Thin foils were prepared as follows: sectioning of 3 mm diameter discs with 400 μm thickness by electrodischarge machining (EDM), mechanically grinding up to 80 μm thickness and final electrolytic thinning by a double-jet electro polisher STRUERS Tenupol-5 (electrolyte: 67% methanol and 33% nitric acid at −30 °C and 10 V). A TEM double tilt holder was used to orientate the thin foils in the (110) plane and dark field images were taken in the [11-1] direction.

Charpy V-notch specimens were sectioned by EDM from hot-rolled alloys. A specimen geometry of 2.5 × 10 × 55 mm^3 (L-T orientation) was adopted based on ASTM Standard E23-18 recommendations for subsize specimens [25]. The final specimen thickness was achieved with a surface grinder. The V-notch was made by EDM after ageing treatments to avoid thermal cracking.

Impact tests were carried out in a Charpy machine equipped with a Joule-effect heating device controlled by a thermocouple welded 3 mm away from the middle of the specimen [26]. The impacts were carried out with a 15 ± 0.1 J hammer, but in some $Fe_{84}Al_8V_8$ samples a higher energy hammer was required (50 ± 0.25 J). The method for determining BDTT and NDT is detailed in the supplementary material.

Dog-bone specimens for hot tensile tests, with a 2 × 2 mm^2 cross-section and 7 mm gauge length, were obtained by a CNC machine. Tensile tests with $\dot{\varepsilon} = 1x10^{-4}s^{-1}$ strain rate were carried out following ASTM Standard E21-20 recommendations [27], in a 10-ton MTS Landmark servo-hydraulic machine. The alloy with the PHC was also tested at $\dot{\varepsilon} = 1x10^{-2}s^{-1}$ and 1 s^{-1}. The temperature was controlled by K-thermocouple (±3 °C) leaning against the specimen centre.

Table 1
Fe–Al base alloys with A2 matrix and strengthened by different precipitate phases ($L2_1$, μ, C14): thermal treatments, average of precipitate radius (r), precipitate volume fraction (θ), average of grain size diameter (d), and brittle-to-ductile transition temperature (BDTT).

Alloy	Thermal treatment	Precipitate phase	r (nm)	θ (%)	d (μm)	BDTT (°C)
$Fe_{76}Al_{12}Ti_{12}$ [12]	700 °C/0.37 h	$L2_1$ (Fe_2AlV)	11	21.8	700	617
$Fe_{69}Al_{21}Ti_{10}$ [7]	As-cast	$L2_1$ (Fe_2AlTi)	5	–	–	925
$Fe_{69}Al_{21}Ti_{10}$ [7]	1000 °C/500 h	$L2_1$ (Fe_2AlTi)	500	–	–	775
$Fe_{74.2}Al_{15.4}Mo_{9.4}$ [13]	1000 °C/200 h	μ (Fe_7Mo_6)	–	2.5	–	600
$Fe_{74.2}Al_{15.0}Mo_{10.9}$ [13]	1000 °C/200 h	μ (Fe_7Mo_6)	–	7.5	–	600
$Fe_{82}Al_{16}Ta_2$ [14]	As-cast	C14 $(Fe,Al)_2Ta$	–	0.9	375	650
$Fe_{81}Al_{16}Ta_3$ [14]	As-cast	C14 $(Fe,Al)_2Ta$	–	10	350	550

Table 3
Alloys microstructure at different thermal treatments. Average precipitate radius (r), grain size (d), brittle-to-ductile transition temperature (BDTT), nil ductility temperature (NDT), yield stress at NDT ($\sigma_{y(NDT)}$) and thermal activation barrier for dislocations glide (σ_{th}^{0}).

Alloy	Phases	Thermal treatment	r (nm)	d (μm)	BDTT (°C)	*NDT* (°C)	$\sigma_{y(NDT)}$ (MPa)	σ_{th}^{0} (MPa)
$Fe_{84}Al_8V_8$	A2			110	154	132	397	340
$Fe_{78}Al_{10}V_{12}$	A2+$L2_1$	700 °C/0.37 h (PHC)	10 ± 2	38	485	470	1029	1080
$Fe_{78}Al_{10}V_{12}$	A2+$L2_1$	700 °C/5 h	29 ± 5	38	409	386	847	845
$Fe_{78}Al_{10}V_{12}$	A2+$L2_1$	700 °C/72 h	61 ± 11	38	341	319	627	600
$Fe_{78}Al_{10}V_{12}$	A2+$L2_1$	GG+700 °C/0.37 h	10 ± 2	75	509	498	1003	1080

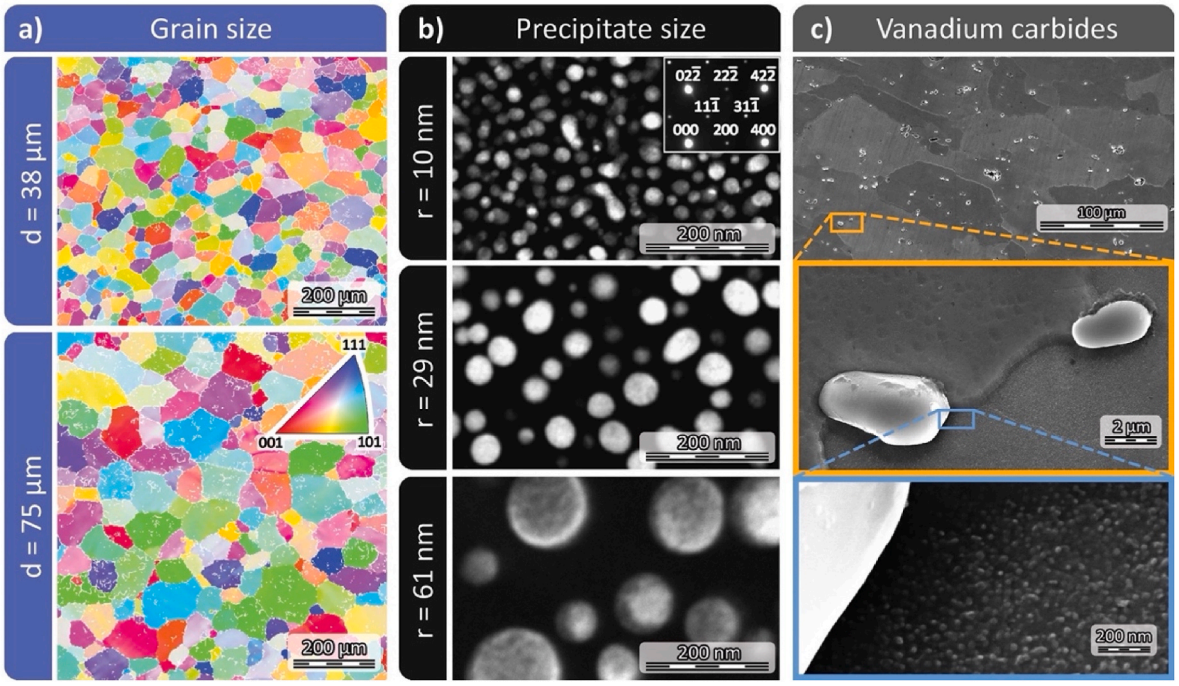

Fig. 1. $Fe_{78}Al_{10}V_{12}$ alloy. (a) EBSD map showing the grain size along the ND-TD section in the hot rolled condition and after GG treatment. (b) TEM dark field $[11\bar{1}]$ taken in the (110) orientation showing the $L2_1$ precipitates in the hot rolled sheet after different ageing times at 700 °C. (c) SEM micrograph showing the distribution of vanadium carbides in the hot-rolled sheet after GG + PHC treatments. Two enlargements are presented: the first shows carbides at grain boundaries and the second shows $L2_1$ precipitates around a carbide.

3. Results and discussion

Table 3 shows the averages of grain diameter (d) and $L2_1$ precipitates radius (r) for the three ageing conditions applied. These precipitate sizes are consistent with the previous reported coarsening rate at 700 °C in a $Fe_{76}Al_{12}V_{12}$ alloy [11] (kinetics in Supplementary material). The distribution of carbides is consistent across the alloy, with a high probability of finding carbides at grain boundaries (Fig. 1c). The carbides size range 1–5 μm, and no size differences between ageing were found.

The absorbed energy versus impact temperature is shown in Fig. 2a and is used to evaluate the BDTT and the *NDT* response for each microstructure (results summarized in Table 3). SEM fractography was performed in each zone of the impact-energy curve for the PHC of $Fe_{78}Al_{10}V_{12}$ alloy (Fig. 2c–e). A ductile fracture with dimples containing carbides inside, a quasi-cleavage pattern of dense dimple regions mixed with cleavage facets, and a cleavage pattern indicated brittle transgranular fracture were observed at 550, 490 and 450 °C, respectively. Using the impact-energy curve of samples with $r = 10$ nm and $d = 38$ μm as reference (Fig. 2a), a clear BDTT increase was seen with increasing grain size, and a decrease by precipitate coarsening. In turn, the single-phase $Fe_{84}Al_8V_8$ alloy showed the lowest BDTT and substantially higher upper shelf energy absorption than the two-phase alloys, and this BDTT value could be assumed as a lower limit for such two-phase alloys. Furthermore, if equivalent hardening of the Fe-matrix by V and Al atoms in solid solution can be considered, the BDTT measurement of the $Fe_{84}Al_8V_8$ alloy agrees with the 100 °C value measured in a $Fe_{83}Al_{17}$ alloy [28].

The measured values of the yield stress $\sigma_{y(NDT)}$ are shown in Table 3. Since the Q factor is a constant, the behaviour of $\sigma_{y(NDT)}$ will reflect that of the cleavage stress. Thus, a lower influence on the cleavage stress due to grain growth is observed with respect to over-ageing. Hall-Petch measurements [29] on various iron and steels, demonstrate that the grain size dependence of the cleavage stress is described as follows:

$$\sigma_c = \sigma_{0c} + k_c d^{-1/2} \quad (1)$$

where σ_{0c} and k_c are constants. Although this relationship is considered as empirical, Petch [30] also argued early that it is consistent with the production of cleavage by the stress concentration ahead of an array of dislocations proportional in length to the grain diameter. The term σ_{0c} represents the stress required simply to move a dislocation, so $(\sigma_c - \sigma_{0c})$ compresses the array. The slope k_c includes the proportionality between the length of the array and the grain diameter and is inversely proportional to the square root of the surface energy to create a cleavage crack [31]. Terlinde and Luetjering [32] were the first to use the Petch's argument modelling the influence of grain size and age-hardening on the tensile fracture of Ti-Al alloys. They found that k_c is independent of grain size and degree of age hardening, while the effective stress compressing

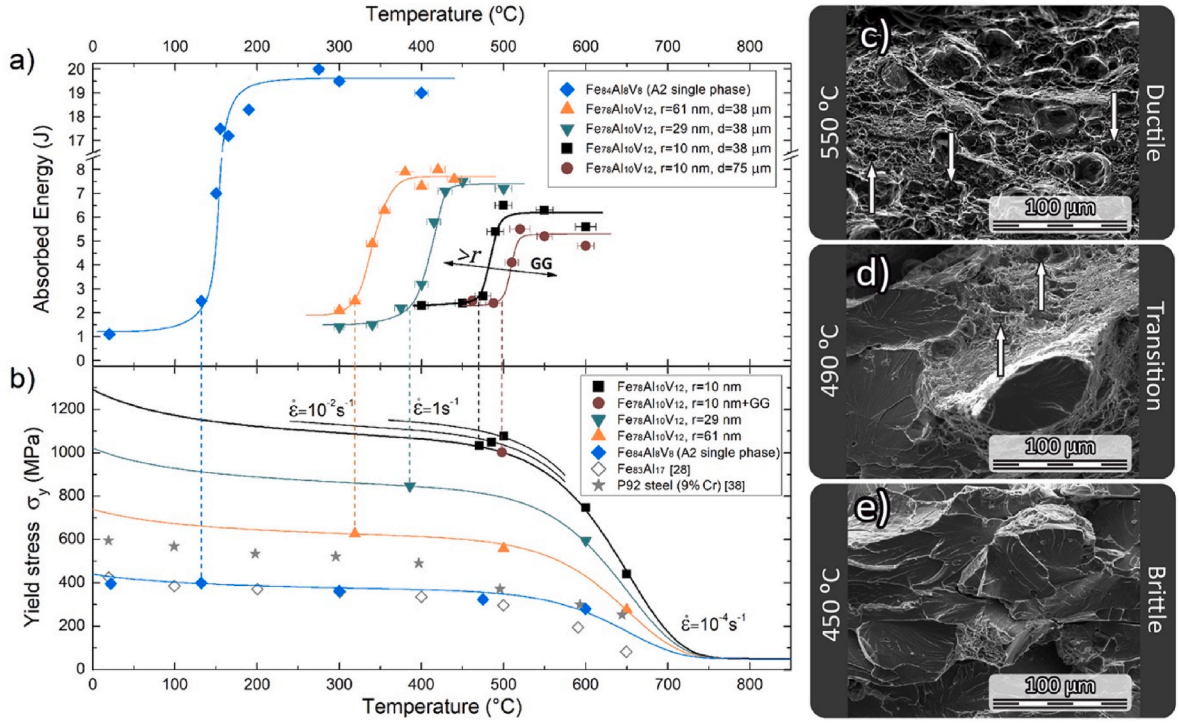

Fig. 2. (a) Absorbed energy against impact test temperatures (dot lines indicate *NDT*). (b) 0.2% yield stresses obtained by hot tensile tests. Lines are fittings of the experimental data using the physical-based model of Eq. (4). SEM fractographies of impacted $Fe_{76}Al_{10}V_{12}$ samples at PHC ($r = 10$ nm and $d = 38$ μm) tested at: (c) 550 °C, (d) 490 °C, and (e) 450 °C. Arrows indicate carbides particles inside of dimples.

the dislocation pile-up is linearly dependent of the particle hardening, $\Delta\sigma_p$, so that Eq. (1) can be rewritten as

$$\sigma_c = \sigma_{0_c}^{SS} + \Delta\sigma_p + k_c d^{-1/2} \tag{2}$$

where $\sigma_{0_c}^{SS}$ is the friction stress required to move a dislocation in the matrix of the particle hardened alloy (see Fig. 3).

According to Eq. (2), the change in cleavage stress, $\Delta\sigma_c$, between the solid solution $Fe_{84}Al_8V_8$ alloy and the age hardened $Fe_{78}Al_{10}V_{12}$ alloy should be as follows

$$\Delta\sigma_c = \Delta\sigma_p + k_c\,\Delta\left(d^{-1/2}\right) \tag{3}$$

Eq. (3) together with the $\sigma_{y(NDT)}$ data (Table 3) allows estimating the effect of grain and precipitate sizes on $\Delta\sigma_c$, but the estimate depends on the Q factor. According to Ref. [20], Q is somewhat smaller than 2.178 as predicted by the slip line field theory for a $(\pi/4)$ notch angle in Charpy specimens. The precipitate size effect on $\Delta\sigma_c$ is showed in Fig. 4a as function of precipitate radius for several values of $Q < 2.178$. The figure considers the model of yield stress increase from particle strengthening that operates in this type of alloy according to our fitting to experimental results from Ref. [11], only the elastic modulus value was decreased to consider the higher testing temperature [33]. As can be seen, the analysis is consistent for different Q factors, however, the $Q = 2$ shows the least scatter between measurements and model. Using this

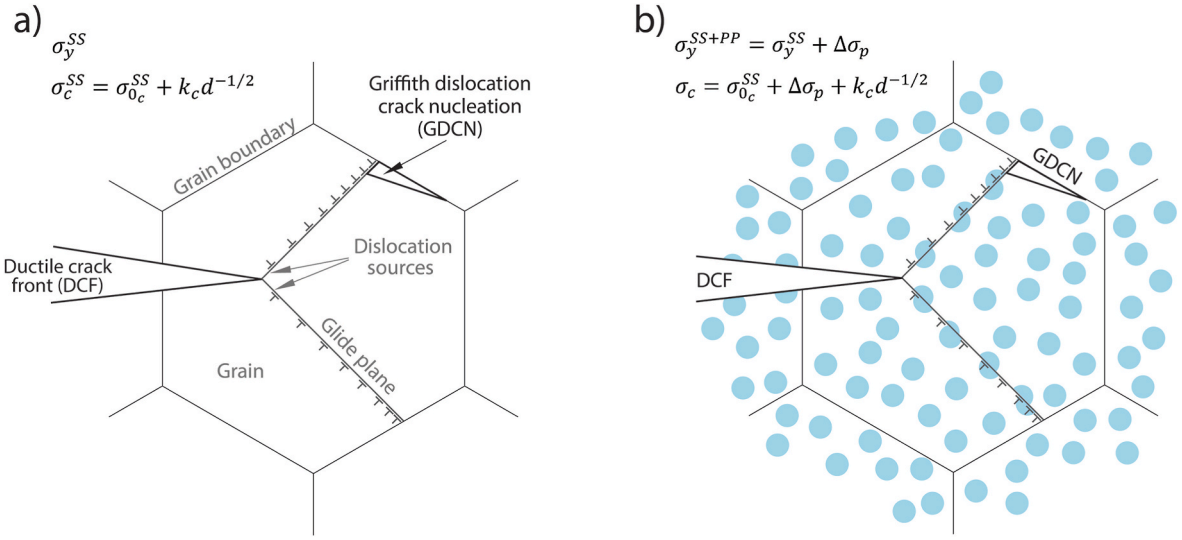

Fig. 3. Schematic representation of the change in cleavage stress when a solid solution (a) is modified by coherent precipitates (b).

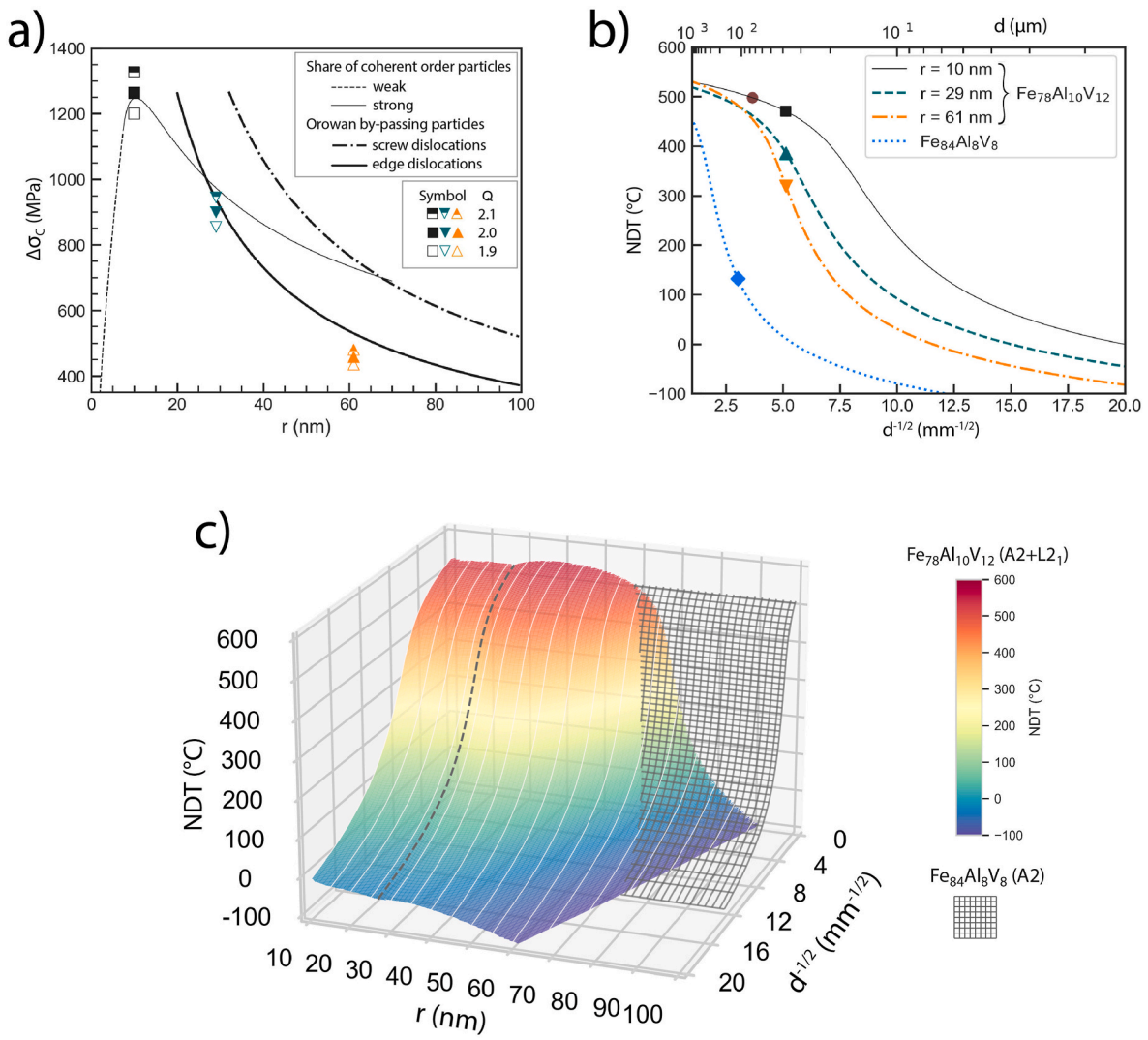

Fig. 4. (a) Change in cleavage stress as function of precipitate radius for three Q values in the $Fe_{76}Al_{10}V_{12}$ alloy with $d = 38$ μm. (b) $NDT(d)$ with experimental data as scatter and physical models, combining Eqs. (2) and (4) with $Q = 2$, as lines. (c) $NDT(d, r)$ surface modelled for the (A2+L2$_1$) $Fe_{76}Al_{10}V_{12}$ alloy, valid above the A2-NDT (gridded surface of $Fe_{84}Al_8V_8$ alloy). The dotted line indicates the dislocation transition from precipitate cutting to Orowan by-passing.

value, the other constants of Eq. (2) were estimated; $\sigma_{0_c}^{SS} = 688\ MPa$ and $k_c = 35.4\ MPa\ mm^{1/2}$. Comparison of these results against those obtained by Petch in iron and steels [29] shows higher σ_{0_c} and lower k_c. The increase of σ_{0_c} can be related to the yield stress raise by solid solution hardening in Fe–Al alloys [28]. The k_c decrease implies that the effective surface energy involved in the formation of new crack faces in the ferritic matrix must increase in some way. The increase in Griffith free energy for cleavage fracture of α-iron due to Al addition [34,35] cannot account for the low k_c observed in our samples with respect to iron and steels. Therefore, the following step is to incorporate the grain boundary carbides, shown in Fig. 1b, in the discussion of cleavage fracture. Almond et al. [36] were pioneers in modelling the initiation of cleavage by cracking of carbide plates at grain boundaries. They obtained the stress to propagate a new ferrite crack formed ahead of the carbide crack, itself produced by a blocked ferrite slip band. The stress was found to depend on both the carbide thickness and the ferrite grain size. Using a different approach, Petch [37] arrived at a similar result and applied it to predict the carbide modification of the grain size dependence of BDTT. At a constant carbide thickness, the predicted cleavage strength is a curve rather than a straight line against $d^{-½}$. However, for grain sizes below 100 μm, the linear representation will be quite close, and the slope k_c decreases as the carbide thickness increases. Based in Petch's calculations [37], using values from physical and mechanical properties of steels, shows that the decrease in k_c estimated for our alloy is consistent with about 2 μm carbide thickness in agreement with the SEM observations.

Since the Q value was estimated together with the influence of grain and precipitate sizes and temperature on σ_c, the relationship $\sigma_c = Q\sigma_{y(NDT)}$ can be used to derive an analytical expression for NDT if the effect of these parameters on σ_y is known. Although several expressions of this type have been proposed and tested for NDT in steels [20,31,37], the authors are not aware of its application in precipitation-hardened ferritic alloys. Fig. 2b shows the behaviour of the yield stress, for different temperatures and strain rates, of the alloys involved in this research (a P92 steel was added for comparison [38]). The highlight in the relation between yield stress and testing temperature is a knee point, above which the magnitude of temperature dependence of yield stress increases sharply. The transition temperature thus evaluated is around 570 °C ($\approx 0.47T_m$, where $T_m = 1804\ K$ is the melting temperature of the alloy estimated by Thermocalc TCNI8 database) at $\dot{\varepsilon}_0 = 10^{-4}\ s^{-1}$.

Under a given dislocations structure, the dislocation motion can be thermally aided and could also be thermally recovered with the aid of applied stress. The former gives the thermal component of flow stress, the latter the temperature dependence of the athermal component of

flow stress. Therefore, both mobility of dislocations and the recovery rate of dislocation structures could give rise to the occurrence of temperature and strain rate dependences of the flow stress. These hypotheses were used successfully by Testa et al. [39] for semi-empirical modelling of the flow stress of bcc metals in a wide range of temperatures and strain rates. The yield stress is given by:

$$\sigma_y = \left(\sigma_{0y} + k_y d^{-1/2}\right) + \sigma_{th}^0 \left[1 + A\exp\left(-\frac{T}{T_1}\right)\right] \times \left[exp\left(-\left(\frac{T}{T_2}\right)^m\right)\right] \times \left[1 + \lambda \ln\left(\frac{\dot{\varepsilon}}{\dot{\varepsilon}_0}\right)\right] \quad (4)$$

The first parenthesis is the Hall-Petch relation, T_1 and T_2 are characteristic temperatures for thermally activation motion of dislocations and for the recovery of dislocation structure, respectively, λ is the sensitivity parameter of strain rate and are dimensionless material constants which characterize the dislocation movement over short barriers. Finally, $\dot{\varepsilon}_0$ is a parameter dependent of: mobile dislocations density, Burger vector, crystal vibration frequency, and temperature by $\dot{\varepsilon}_0 = 10^6 (T/T_m)^m \, s^{-1}$.

Samples with different grain sizes and PHC ageing, were prepared to estimate the Hall-Petch coefficients of yield stress by hardness test. Contrary to expectations, the increase in grain size between 50 and 130 μm did not lead to an appreciable decrease in hardness, therefore the sensitivity of σ_y to grain size is negligible against precipitation hardening ($k_y \ll \sigma_{th}^0$). Then, to calibrate the model to our experimental data at different strain rates, temperature, and precipitate size, it was required to estimate seven parameters. The fitting procedure has been performed as follow. First, a non-linear fit of Eq. (4) was performed to the yield stress data as a function of temperature for $\dot{\varepsilon}_0 = 10^{-4} \, s^{-1}$, the only parameter that varies with the precipitate size is σ_{th}^0. Second, the value of the parameter λ was refined by fitting the σ_y data as a function of $\dot{\varepsilon}_0$ for $r = 10$ nm. The following estimates were found $(\sigma_{0y} + k_y d^{-1/2}) =$ 50 MPa; $A = 3.5$; $m = 16$; $T_1 = 75$ K; $T_2 = 930$ K; $\lambda = 755x10^{-5}$ and σ_{th}^0 values are given in Table 3. The fitted curves can be seen in Fig. 2b.

Now, by combining the stress criterion for the brittle-ductile transition with Eqs. (2) and (4), we obtain the *NDT* as a function of grain and precipitate sizes. Thus, in Fig. 4b, the *NDT* vs grain size curves are compared against the data obtained for the alloys. Going further, and assuming a linear dependence of σ_{th}^0 on the precipitate radius, it is possible to plot the surface $NDT(d, r)$ (Fig. 4c). This surface is valid only when the *NDT* of the ferritic matrix is lower (gridded surface). It can be noted that the model predicts a large influence of precipitate size to reduce the *NDT* when the grain size becomes smaller.

4. Conclusion

This study has shown aspects of the cleavage fracture stress and yield stress in a two-phase coherent strengthened bcc Fe–Al–V alloy. In particular, the same behaviour of the increase in yield stress by coherent strengthening precipitation was observed in the increase of cleavage stress. This last result is not obvious and has not been previously published. To achieve this result, an evaluation of the change in the cleavage stress between a single-phase and a two-phase alloys, whose connecting phase has the same crystal structure and chemical composition, was required. Moreover, the effect of grain growth and precipitate coarsening on this change in cleavage stress was explored, which allowed access to the null ductility temperature relation, $NDT(d, r)$, and thus obtain a powerful strategy to minimize the brittle-to-ductile transition temperature (BDTT). Finally, the applied physical-based methodology provides enhanced predictive capability to accelerate the design & development of bcc-superalloys.

CRediT authorship contribution statement

P.A. Ferreirós: Conceptualization, Methodology, Investigation, Formal analysis, Writing – original draft, Writing – review & editing, Visualization, Supervision, Funding acquisition. **U.A. Sterin:** Conceptualization, Methodology, Investigation, Formal analysis, Writing – original draft, Writing – review & editing. **P.R. Alonso:** Writing – review & editing, Supervision, Funding acquisition. **A.J. Knowles:** Writing – review & editing, Funding acquisition, Project administration. **G.H. Rubiolo:** Conceptualization, Supervision, Writing – original draft, Writing – review & editing, Funding acquisition, Project administration.

Declaration of competing interest

The authors declare that they have no known competing financial interests or personal relationships that could have appeared to influence the work reported in this paper.

Data availability

Data will be made available on request.

Acknowledgements

The authors gratefully acknowledge the Centre for Electron Microscopy (University of Birmingham) for their support & assistance in this work. This research used internal founding of the Comisión Nacional de Energía Atómica. A.J. Knowles gratefully acknowledges funding from EPSRC [EP/T016566/1], UKRI Future Leaders Fellowship [MR/T019174/1] and Royal Academy of Engineering Research Fellowship, UK. U.A. Sterin was supported by Instituto Sabato & CONICET fellowships.

Appendix A. Supplementary data

Supplementary data to this article can be found online at https://doi.org/10.1016/j.msea.2022.144031.

References

[1] R. Viswanathan, J.F. Henry, J. Tanzosh, G. Stanko, J. Shingledecker, B. Vitalis, R. Purgert, U.S. program on materials technology for ultra-supercritical coal power plants, J. Mater. Eng. Perform. 14 (2005) 281–292, https://doi.org/10.1361/10599490524039.
[2] H.K.D.H. Bhadeshia, Design of ferritic creep-resistant steels, ISIJ Int. 41 (2001) 626–640, https://doi.org/10.2355/isijinternational.41.626.
[3] F. Masuyama, History of power plants and progress in heat resistant steels, ISIJ Int. 41 (2001) 612–625, https://doi.org/10.2355/isijinternational.41.612.
[4] C. Stallybrass, A. Schneider, G. Sauthoff, The strengthening effect of (Ni,Fe)Al precipitates on the mechanical properties at high temperatures of ferritic Fe–Al–Ni–Cr alloys, Intermetallics 13 (2005) 1263–1268, https://doi.org/10.1016/j.intermet.2004.07.048.
[5] M. Palm, Concepts derived from phase diagram studies for the strengthening of Fe–Al-based alloys, Intermetallics 13 (2005) 1286–1295, https://doi.org/10.1016/j.intermet.2004.10.015.
[6] D.G. Morris, M.A. Muñoz-Morris, L.M. Requejo, C. Baudin, Strengthening at high temperatures by precipitates in Fe-Al-Nb alloys, Intermetallics 14 (2006) 1204–1207, https://doi.org/10.1016/j.intermet.2005.10.015.
[7] R. Krein, M. Palm, M. Heilmaier, Characterization of microstructures, mechanical properties, and oxidation behavior of coherent A2 + $L2_1$ Fe-Al-Ti, J. Mater. Res. 24 (2009) 3412–3421, https://doi.org/10.1557/jmr.2009.0403.
[8] P. Hanus, E. Bartsch, M. Palm, R. Krein, K. Bauer-Partenheimer, P. Janschek, Mechanical properties of a forged Fe-25Al-2Ta steam turbine blade, Intermetallics 18 (2010) 1379–1384, https://doi.org/10.1016/j.intermet.2009.12.035.
[9] Z.K. Teng, F. Zhang, M.K. Miller, C.T. Liu, S. Huang, Y.T. Chou, R.H. Tien, Y. A. Chang, P.K. Liaw, New NiAl-strengthened ferritic steels with balanced creep resistance and ductility designed by coupling thermodynamic calculations with focused experiments, Intermetallics 29 (2012) 110–115, https://doi.org/10.1016/j.intermet.2012.05.007.
[10] P.A. Ferreirós, P.R. Alonso, P.H. Gargano, P.B. Bozzano, H.E. Troiani, A. Baruj, G. H. Rubiolo, Characterization of microstructures and age hardening of $Fe_{1-2x}Al_xV_x$ alloys, Intermetallics 50 (2014) 65–78, https://doi.org/10.1016/j.intermet.2014.02.014.

[11] P. A Ferreirós, P.R. Alonso, G.R. Rubiolo, Coarsening process and precipitation hardening in Fe_2AlV-strengthened ferritic $Fe_{76}Al_{12}V_{12}$ alloy, Mater. Sci. Eng., A 684 (2017) 394–405, https://doi.org/10.1016/j.msea.2016.12.074.
[12] P. A Ferreirós, P.R. Alonso, G.R. Gomez, G.H. Rubiolo, Impact toughness transition temperature of ferritic Fe-Al-V alloy with strengthening Fe_2AlV precipitates, Mater. Sci. Eng., A 706 (2017) 136–141, https://doi.org/10.1016/j.msea.2017.09.001.
[13] M. Eumann, M. Palm, G. Sauthoff, Iron-rich iron-aluminium-molybdenum alloys with strengthening intermetallic μ phase and R phase precipitates, Steel Res. Int. 75 (2004) 62–73, https://doi.org/10.1002/srin.200405928.
[14] D.D. Risanti, G. Sauthoff, Strengthening of iron aluminide alloys by atomic ordering and Laves phase precipitation for high-temperature applications, Intermetallics 13 (2005) 1313–1321, https://doi.org/10.1016/j.intermet.2004.12.029.
[15] T. Śmida, V. Magula, Brittle to ductile transition – an engineer's point of view, Mater. Des. 54 (2014) 582–586, https://doi.org/10.1016/j.matdes.2013.08.039.
[16] W. W Gerberich, K. M Schmalbach, Y. Chen, E. Hintsala, N.A. Mara, Quantifying physical parameters to predict brittle/ductile behavior, Mater. Sci. Eng., A 808 (2021), 140899, https://doi.org/10.1016/j.msea.2021.140899.
[17] B.-S. Li, T.J. Marrow, D.E.J. Armstrong, Measuring the brittle-to-ductile transition temperature of tungsten–tantalum alloy using chevron-notched micro-cantilevers, Scripta Mater. 180 (2020) 77–82, https://doi.org/10.1016/j.scriptamat.2020.01.030.
[18] V. Shah, J.A.W. van Dommelen, E. Altstadt, A. Das, M.G.D. Geers, Brittle-ductile transition temperature of recrystallized tungsten following exposure to fusion relevant cyclic high heat load, J. Nucl. Mater. 541 (2020), 152416, https://doi.org/10.1016/j.jnucmat.2020.152416.
[19] C. Bonnekoh, A. Hoffmann, J. Reiser, The brittle-to-ductile transition in cold rolled tungsten: on the decrease of the brittle-to-ductile transition by 600 K to − 65 °C, Int. J. Refract. Met. Hard Mater. 71 (2018) 181–189, https://doi.org/10.1016/j.ijrmhm.2017.11.017.
[20] R.W. Armstrong, The influence of polycrystal grain size on several mechanical properties of materials, Metall. Mater. Trans. B 1 (1970) 1169–1176, https://doi.org/10.1007/BF02900227.
[21] R. Sandström, Y. Bergström, Relationship between Charpy V transition temperature in mild steel and various material parameters, Met. Sci. 18 (1984) 177–186, https://doi.org/10.1179/030634584790420203.
[22] A. Michalcová, L. Senčekova, G. Rolink, A. Weisheit, J. Pešička, M. Stobik, M. Palm, Laser additive manufacturing of iron aluminides strengthened by ordering, borides or coherent Heusler phase, Mater. Des. 116 (2017) 481–494, https://doi.org/10.1016/j.matdes.2016.12.046.
[23] P. A Ferreirós, P.R. Alonso, G.H. Rubiolo, Effect of Ti additions on phase transitions, lattice misfit, coarsening, and hardening mechanisms in a Fe_2AlV-strengthened ferritic alloy, J. Alloys Compd. 806 (2019) 683–697, https://doi.org/10.1016/j.jallcom.2019.07.288.
[24] P.R. Alonso, P.H. Gargano, P.B. Bozzano, G.E. Ramírez-Caballero, P.B. Balbuena, G. H. Rubiolo, Combined ab initio and experimental study of $A2 + L2_1$ coherent equilibria in the Fe–Al–X (X = Ti, Nb, V) systems, Intermetallics 19 (2011) 1157–1167, https://doi.org/10.1016/j.intermet.2011.03.025.
[25] ASTM Standard E23-18, Standard Test Methods for Notched Bar Impact Testing of Metallic Materials, ASTM International., West Conshohocken, Philadelphia (PA), 2018.
[26] P.A. Ferreirós, P.R. Alonso, P.H. Gargano, G.H. Rubiolo, High-temperature testing in a Charpy impact pendulum using in-situ Joule heating of the specimen, Fatig. Fract. Eng. Mater. Struct. 41 (2018) 1171–1182, https://doi.org/10.1111/ffe.12761.
[27] Astm Standard E21-20, Standard Test Methods for Elevated Temperature Tension Tests of Metallic Materials, ASTM International, West Conshohocken, Philadelphia (PA), 2017.
[28] J. Herrmann, G. Inden, G. Sauthoff, Deformation behaviour of iron-rich iron-aluminium alloys at high temperatures, Acta Mater. 51 (2003) 3233–3242, https://doi.org/10.1016/S1359-6454(03)00144-7.
[29] N.J. Petch, The cleavage strength of polycrystals, J. Iron Steel Inst. 174 (1953) 25–28.
[30] N.J. Petch, XVI. The ductile fracture of polycrystalline α-iron, Philos. Mag. A 1 (1956) 186–190, https://doi.org/10.1080/14786435608238091.
[31] N.J. Petch, The ductile-brittle transition in the fracture of α-iron: I, Philos. Mag. A 3 (1958) 1089–1097, https://doi.org/10.1080/14786435808237038.
[32] G. Terlinde, G. Luetjering, Influence of grain size and age-hardening on dislocation pile-ups and tensile fracture for a Ti-ai alloy, Metall. Trans. A 13 (1982) 1283–1292, https://doi.org/10.1007/BF02645512.
[33] W. Köster, T. Gödecke, Physikalische Messungen an Eisen-Aluminium-Legierungen mit 10 bis 50 At.-% Al, Z. Metallkd. 73 (1982) 111–114.
[34] J.J. Möller, E. Bitzek, Comparative study of embedded atom potentials for atomistic simulations of fracture in α-iron, Model. Simulat. Mater. Sci. Eng. 22 (2014), 045002, https://doi.org/10.1088/0965-0393/22/4/045002.
[35] R. Besson, M. Biscondi, J. Morillo, Interfaces in iron-rich ordered Fe-Al alloys: an atomic-scale simulation study, Interface Sci. 7 (1999) 103–117, https://doi.org/10.1023/A:1008727517535.
[36] E.A. Almond, D.H. Timbres, J.D. Embury, Fracture in quench-aged low-carbon steels, Can. Metall. Q. 8 (1969) 51–58, https://doi.org/10.1179/cmq.1969.8.1.51.
[37] N.J. Petch, The influence of grain boundary carbide and grain size on the cleavage strength and impact transition temperature of steel, Acta Metall. 34 (1986) 1387–1393, https://doi.org/10.1016/0001-6160(86)90026-X.
[38] F. Peñalba, X. Gómez-Mitxelena, J.A. Jiménez, M. Carsí, O.A. Ruano, Effect of temperature on mechanical properties of 9% Cr ferritic steel, ISIJ Int. 56 (2016) 1662–1667, https://doi.org/10.2355/isijinternational.ISIJINT-2016-097.
[39] G. Testa, N. Bonora, A. Ruggiero, G. Lannitti, Flow stress of bcc metals over a wide range of temperature and strain rates, Metals 10 (2020) 120, https://doi.org/10.3390/met10010120.